Comparing Effective One Body gravitational waveforms to accurate numerical data

T. DAMOUR and A. NAGAR

Comparing Effective-One-Body gravitational waveforms to accurate numerical data

Thibault Damour[1,2] and Alessandro Nagar[*1,2]

[1]*Institut des Hautes Etudes Scientifiques, 91440 Bures-sur-Yvette, France*
[2]*ICRANet, 65122 Pescara, Italy*
(Dated: January 22, 2008)

We continue the program of constructing, within the Effective-One-Body (EOB) approach, high accuracy, faithful analytic waveforms describing the gravitational wave signal emitted by inspiralling and coalescing binary black holes. We present the comparable-mass version of a new, *resummed* 3 PN-accurate EOB quadrupolar waveform that we recently introduced in the small-mass-ratio limit. We compare the phase and the amplitude of this waveform to the recently published results of a high-accuracy numerical simulation of 15 orbits of an inspiralling equal-mass binary black hole system performed by the Caltech-Cornell group. We find a remarkable agreement, both in phase and in amplitude, between the new EOB waveform and the published numerical data. More precisely: (i) in the gravitational wave (GW) frequency domain $M\omega < 0.08$ where the phase of one of the non-resummed "Taylor approximant" (T4) waveform matches well with the numerical relativity one, we find that the EOB phase fares as well, while (ii) for higher GW frequencies, $0.08 < M\omega \lesssim 0.14$, where the Taylor T4 approximant starts to significantly diverge from the numerical relativity phase, we show that the EOB phase continues to match well the numerical relativity one. We further propose various methods of tuning the two inspiral flexibility parameters, a_5 and $v_{\rm pole}$, of the EOB waveform so as to "best fit" EOB predictions to numerical data. We find that the maximal dephasing between EOB and numerical relativity can then be reduced below 10^{-3} GW cycles over the entire span (30 GW cycles) of the simulation (while, without tuning them, the dephasing is $< 8 \times 10^{-3}$ cycles). In addition, our resummed EOB amplitude agrees much better with the numerical relativity one than any of the previously considered non-resummed, post-Newtonian one (including a recently derived, non-resummed 3 PN-accurate one). We think that the present work, taken in conjunction with other recent works on the EOB-numerical-relativity comparison confirms the ability of the EOB formalism (especially in its recently improved avatars) to faithfully capture the "real" general relativistic waveforms.

PACS numbers: 04.25.Nx, 04.30.-w, 04.30.Db

I. INTRODUCTION

A ground-based network of interferometric gravitational wave (GW) detectors is currently taking data. Coalescing black hole binaries are among the most promising GW sources for these detectors. In order to successfully detect GWs from coalescing black hole binaries and to be able to reliably measure the source physical parameters, one needs to have in advance a large bank of "*templates*" that accurately represent the GW waveforms emitted by these binaries. In the terminology of [1] one needs templates that are both *effectual* and *faithful*. The construction of faithful GW templates for coalescing binaries comprising spinning black holes (with arbitrary masses m_1, m_2 and spins $\mathbf{S}_1$, $\mathbf{S}_2$) poses a difficult challenge. Due to the multi-dimensionality of the corresponding parameter space, it seems impossible for state-of-the-art numerical simulations to densely sample this parameter space. This motivates the need to develop *analytical* methods for computing (as a function of the physical parameters m_1, m_2, $\mathbf{S}_1$, $\mathbf{S}_2$) the corresponding waveforms. The Effective-One-Body (EOB) method [2–

5] was developed to analytically represent the motion of, and radiation from, coalescing binary black holes with arbitrary masses and spins. As early as 2000 [3] this method made several quantitative and qualitative predictions concerning the dynamics of the coalescence, and the corresponding waveform, notably: (i) a blurred transition from inspiral to a "plunge" that is just a smooth continuation of the inspiral, (ii) a sharp transition, around the merger of the black holes, between a continued inspiral and a ringdown signal, and (iii) estimates of the radiated energy and of the spin of the final black hole.

The recent impressive breakthroughs in numerical relativity (NR) [6–20] have given us access to extremely valuable, and reliable, information about the dynamics and radiation of binary black hole coalescence. It is comforting (for theorists) to note that the picture which is emerging from the recent numerical simulations (for a review see [21]) broadly confirms the predictions made by the EOB approach. This gives us confidence in the soundness of the various theoretical tools and assumptions used in this approach, such as the systematic use of *resummation* methods, notably Padé approximants (as first suggested in [1]).

An important aspect of the EOB approach (which was emphasized early on [5]) is its *flexibility*. As was mentioned in the latter reference "one can modify the basic functions [such as $A(u)$] determining the EOB dy-

namics by introducing new parameters corresponding to (yet) uncalculated higher PN effects.[...]. Therefore, when either higher-accuracy analytical calculations are performed or numerical relativity becomes able to give physically relevant data about the interaction of (fast-spinning) black holes, we expect that it will be possible to complete the current EOB Hamiltonian so as to incorporate this information". Several aspects of the EOB flexibility have been investigated early on, such as a possible "fitting" of a parameter (here denoted as a_5), representing unknown higher PN effects, to numerical relativity data [22] concerning quasi-equilibrium initial configurations [23, 24], and the extension of the EOB formalism by several new "flexibility parameters" [25], and notably a parameter, here denoted as v_{pole}, entering the Padé resummation of the (energy flux and) radiation reaction force.

In view of the recent progress in numerical relativity, the time is ripe for tapping the information present in numerical data, and for using it to *calibrate* the various flexibility parameters of the EOB approach. This general program has been initiated in a series of recent papers which used 3-dimensional numerical relativity results [26–29]. In addition, numerical simulations of test particles (with an added radiation reaction force) moving in black hole backgrounds have given an excellent (and well controllable) "laboratory" for learning various ways of improving the EOB formalism by comparing it to numerical data [30]. The latter work has introduced a new *resummed* 3 PN-accurate quadrupolar waveform which was shown to exhibit a remarkable agreement with "exact" waveforms (in the small mass ratio limit). In the present paper, we shall present the comparable-mass version of our new, resummed 3 PN-accurate quadrupolar waveform and compare it to the published results [20] concerning recent high-accuracy numerical simulation of 15 orbits of an inspiralling equal-mass binary black hole system. We then show how the agreement between the two (which is quite good even without any tuning) can be further improved by tuning the two main EOB flexibility parameters: a_5 and v_{pole}. Our work will give new evidence for the remarkable ability of the EOB formalism at describing, in fine quantitative details, the waveform emitted by a coalescing binary.

II. CALIBRATING v_{pole}, IN THE SMALL-MASS-RATIO CASE, FROM NUMERICAL DATA

As a warm up towards our comparable-mass flexibility study, let us first consider the much simpler small-mass-ratio case, $\nu \ll 1$. Here, ν denotes the symmetric mass ratio $\nu = m_1 m_2/(m_1 + m_2)^2$ of a binary system of non-spinning black holes, with masses m_1 and m_2. We also denote $M = m_1 + m_2$ ("total rest mass"), and $\mu = m_1 m_2/M$ ("effective mass for the relative motion"), so that $\nu = \mu/M$. In the small-mass-ratio limit

$\nu \ll 1$, the conservative dynamics of the small mass (say $m_2 \simeq \mu$) around the large one ($m_1 \simeq M$) is known, being given by the Hamiltonian describing a test particle μ in the background of a Schwarzschild black hole of mass M. On the other hand, the energy flux toward infinity, say $F = (dE/dt)^{rad}$, or the associated radiation reaction force $\mathcal{F}_{RR}$, cannot be analytically computed in closed form. One must resort to black hole perturbation theory, whose foundations were laid down long ago by Regge and Wheeler [31], and by Zerilli [32] (for the non-spinning case considered here). The waveform emitted by a test particle is then computed by solving decoupled partial differential equations (for each multipolarity (ℓ, m) of even or odd parity π) of the form

$$\partial_t^2 h_{\ell m}^{(\pi)} - \partial_{r_*}^2 h_{\ell m}^{(\pi)} + V_\ell^{(\pi)}(r_*)h_{\ell m}^{(\pi)} = S_{\ell m}^{(\pi)} , \qquad (1)$$

where $V_\ell^{(\pi)}$ is an effective radial potential and where the source term $S_{\ell m}^{(\pi)}$ [32–34] is linked to the dynamics[1] of $m_2 \simeq \mu$ around $m_1 \simeq M$.

At this stage we have two options for solving Eq. (1): (i) use numerical methods, or (ii) use an analytical approximation scheme for solving (1) by successive approximations. The numerical approach led, long ago, to the discovery of several important features of gravitational radiation in black hole backgrounds, such as the sharp transition between the plunge signal and a ringing tail when a particle falls into a black hole [36]. The analytical approach to solving Eq. (1) by successive approximations, of the post-Newtonian (PN) type, has been recently driven to unprecedented heights of sophistication (and iteration order). See [37] for a review.

Our purpose in this introductory section is to illustrate, on a simple case, how accurate numerical data can be used to optimize the resummation of PN-expanded analytical results. We consider the case of a particle on a circular orbit. The numerical solution of this problem [38, 39] leads to an accurate knowledge of the radiated energy flux F as a function of the orbital radius, or equivalently (and more invariantly) of the "velocity parameter" $v = (GM\Omega)^{1/3}$. See Fig. 1 where the solid ("Exact") line represent the "Newton-normalized flux function"

$$\hat{F}(v) \equiv \frac{F(v)}{F_N(v)}; \quad \text{with} \quad F_N(v) \equiv \frac{32}{5}\nu^2 v^{10} . \qquad (2)$$

On the other hand, post-Newtonian perturbation theory allows one to compute $\hat{F}(v)$ as, essentially, a *Taylor*

---

[1] As discussed in [30, 35] the small-mass-ratio limit of the EOB formalism leads to a generalization of the Regge-Wheeler-Zerilli formalism in that the dynamics of the sourcing particle μ is not taken to be geodesic, but is assumed to be modified by a radiation reaction force $\mathcal{F}_{RR}$. The main issue of interest here is to optimize the resummation of the analytical approximation to $\mathcal{F}_{RR}$, which is given by a badly convergent post-Newtonian expansion (known only to some finite order).

series in powers of v (modulo the appearance of logarithms of v in the coefficients A_n when $n \geq 6$, except for $n = 7$) [37], say

$$\hat{F}^{\mathrm{Taylor}}(v) = 1 + A_2 v^2 + A_3 v^3 + \cdots + A_n v^n + \cdots . \quad (3)$$

It was emphasized by Poisson [39] that the successive Taylor approximants obtained from Eq. (3) converge both slowly and erratically to the numerically determined "exact" $\hat{F}(v)$. Subsequently, Ref. [1] pointed out that the resummation of the series (3) by means of successive (near diagonal) *Padé approximants* led to a much better sequence of approximants. See Fig. 3 in Ref. [1] for a comparison between Taylor approximants and Padé approximants. The convergence of the sequence of Padé approximants was found to be much improved (the v^5 approximant being already very close to all its successors), and to be monotonic. This led to the suggestion of using such Padé approximants also in the comparable-mass case, though we do not know (yet) the finite-ν analog of the exact flux function $F(v; \nu)$.

The Padé resummation advocated in Ref. [1] involves one *flexibility parameter*, v_{pole}, which parametrizes the location of the (real and positive) pole of the Padé-resummed $\hat{F}^{\mathrm{Pade}}(v, v_{\mathrm{pole}})$ which is closest to the origin in the complex v plane. Technically speaking, $\hat{F}^{\mathrm{Pade}}(v; v_{\mathrm{pole}})$ is defined as $(1 - v/v_{\mathrm{pole}})^{-1}$ times the relevant near-diagonal Padé approximant [2] of the $v_{\mathrm{pole}} - modified$ Taylor series $\hat{F}'^{\mathrm{Taylor}}(v, v_{\mathrm{pole}}) \equiv \hat{F}^{\mathrm{Taylor}}(v) - (v/v_{\mathrm{pole}})\hat{F}^{\mathrm{Taylor}}(v) = 1 - v/v_{\mathrm{pole}} + A_2 v^2 + \cdots$. Ref. [1] advocated to use, as a fiducial value for v_{pole}, $v_{\mathrm{pole}} = 1/\sqrt{3} = 0.57735$ in the test-mass limit $\nu \to 0$, and a slightly larger, ν-dependent value, say $v_{\mathrm{pole}}^{\mathrm{DIS}}(\nu)$ (motivated by Padé resumming an auxiliary "energy function" $e(v; \nu)$) given in Eq. (4.8) there. Here, we point out that, when $\nu \to 0$, a slightly different choice for the numerical value of v_{pole} can very significantly improve the closeness between the Padé flux and the exact (numerical) one.

Our results are displayed in Fig 1 (a) and (b). In both panels, the solid line represents the "exact" result for the flux function $\hat{F}(v)$ as numerically computed by Poisson. In the upper part of Fig 1 (a) one compares $\hat{F}^{\mathrm{Exact}}(v)$ to two different Padé (P_6^5) approximants resumming the same v^{11}-accurate (or 5.5 PN) Taylor approximant [40]: the "standard" $\hat{F}^{\mathrm{Pade}}(v; v_{\mathrm{pole}} = 1/\sqrt{3})$ and a "v_{pole}-flexed" [25] version of $\hat{F}^{\mathrm{Pade}}(v; v_{\mathrm{pole}})$ using the optimized value $v_{\mathrm{pole}}^{\mathrm{best}}(5.5\mathrm{PN}) = 0.5398$. This choice of v_{pole} yields a Padé approximant which is amazingly close to the exact value. The lower panel of Fig 1

(a) exhibits the differences $\Delta = \hat{F}^{\mathrm{Pade}} - \hat{F}^{\mathrm{Exact}}$ for the two choices of v_{pole}. While the standard choice of v_{pole} (namely $1/\sqrt{3} = 0.57735$) leads to a rather good agreement (with $|\Delta|$ being smaller than 5×10^{-3} up to $v \simeq 0.355$, which corresponds to a radius $r = 7.93 GM$, and $|\Delta|$ reaching 2.4×10^{-2} at the Last Stable Orbit (LSO) at $r = 6GM$), the "flexed choice" $v_{\mathrm{pole}}^{\mathrm{best}} = 0.5398 \pm 0.0001$ yields an amazing agreement all over the interval $0 \leq v \leq v_{\mathrm{LSO}} = 1/\sqrt{6} = 0.40825$. The largest value of $|\Delta|$ over this interval is $\max |\Delta| \simeq 9 \times 10^{-4}$, and is reached around $v = 0.38$. Note that the 4-digit accuracy quoted for $v_{\mathrm{pole}}^{\mathrm{best}} = 0.5398 \pm 0.0001$ corresponds to (somewhat arbitrarily) imposing that the value of $|\Delta|$ at the LSO is smaller than about 1×10^{-4}. The rounded off value $v_{\mathrm{pole}} = 0.54$ would still yield an amazing fit with $\max |\Delta| \simeq 10^{-3}$.

In Fig. 1 (b) we explore what happens when using a much lower accuracy for the Taylor approximant of the flux. We consider here, as an example of relevance for the finite ν case, the case where one starts from a v^6-accurate (3PN) Taylor approximant for the flux[3]. For that case the standard-choice $v_{\mathrm{pole}} = 1/\sqrt{3}$ still leads to a rather good agreement (with $|\Delta| < 10^{-2}$ up to $v \simeq 0.325$ and $|\Delta|_{\mathrm{LSO}} \simeq 5 \times 10^{-2}$), while the flexed choice $v_{\mathrm{pole}}^{\mathrm{best}} = 0.53$ yields an excellent agreement all over the interval $0 \leq v \leq v_{\mathrm{LSO}}$ (with $\max |\Delta| \simeq 3 \times 10^{-3}$ being reached around $v \simeq 0.355$). Though the closeness is less good than in the 5.5 PN case (3×10^{-3} versus 0.9×10^{-3}), it is even more amazing to think that, starting from a 3PN-expanded flux function which (as shown, e.g., in Fig. 3 of Ref. [1]) differs from the exact result when $0.3 \lesssim v \lesssim v_{\mathrm{LSO}}$ by about 10%, a suitably flexed Padé resummation can decrease the difference below the 3×10^{-3} level!

Summarizing: In the small ν limit, the value of the flexibility parameter v_{pole} can be calibrated to yield an excellent agreement (from 3×10^{-3} to 0.9×10^{-3} depending on the PN accuracy) between the Padéed flux function $\hat{F}^{\mathrm{Pade}}(v; v_{\mathrm{pole}})$ and the numerically determined "exact" flux $\hat{F}^{\mathrm{Exact}}(v)$ all over the interval $0 \leq v \leq v_{\mathrm{LSO}}$. This gives an example of the use of accurate numerical data to calibrate a theoretical flexibility parameter entering the EOB approach. In the following, we shall consider the equal-mass case, $\nu = 1/4$, and investigate to what extent accurate numerical data [20] can be similarly used to calibrate the two main EOB flexibility parameters a_5 and v_{pole}[4].

---

[2] Given a certain order for the Taylor approximant, say $\hat{F}'^{\mathrm{Taylor}} = 1 + \cdots + v^N$, the general prescription is to resum it with a *near-diagonal* Padé, P_n^m, such that $m + n = N$ and $n = m + \epsilon$ with $\epsilon = 0$ or 1. In the (exceptional) cases where such a near-diagonal Padé contains a "spurious pole" (i.e., a real pole between 0 and v_{pole}), one should use another choice for m and n (staying as close as possible to the diagonal $m = n$).

[3] The result for the v^7-accurate expansion would be very similar and the final difference would be invisible to the naked eye. However, as we shall mention below, some problems with spurious poles creep up in the near diagonal 3.5 PN Padé approximant when $\nu = 1/4$ and $v_{\mathrm{pole}} \leq 0.55$. Therefore we prefer to exhibit here the spurious-pole-free 3 PN Padé case.

[4] Note that, as already suggested in Ref. [1], one expects the "true" value of v_{pole} to depend on ν. Therefore, we cannot a priori assume that the above best values, say $v_{\mathrm{pole}}^{\mathrm{best}} \simeq 0.53$, will yield a close agreement for the flux function (or the radiation reaction)

III. NEW, RESUMMED 3 PN-ACCURATE EOB INSPIRAL WAVEFORM

After having considered the importance, for fitting high-accuracy numerical data, of the flexibility parameter v_{pole} in the simpler small-mass-ratio limit, we wish to move on to the observationally urgent comparable mass case $4\nu \sim 1$. As we are going to see, this case involves *two*, rather than one, relevant flexibility parameters: v_{pole} (entering radiation reaction) and a_5 (entering the conservative orbital dynamics). To understand the meaning of these parameters when $4\nu \sim 1$, let us present the comparable-mass version of the new, improved "version" of EOB which has been introduced in Ref. [30] and shown there to exhibit a remarkable agreement, in phase and in amplitude, with "exact" small mass ratio NR waveforms. Ref. [30] considered the small ν limit, but with the clear methodological aim of using this limit to test improved EOB waveforms defined for any value of ν. We here continue this program by comparing this improved EOB waveform to the recent numerical relativity data of [20]. The improvements in the EOB approach introduced in Ref. [30] concern several of the separate "bricks" entering this approach. Indeed, it included: (i) a resummed, 3 PN-accurate description of the inspiral waveform, (ii) a better description of radiation reaction during the plunge, (iii) a refined analytical expression of the plunge waveform, and (iv) an improved treatment of the matching between the plunge and ring-down waveforms. As the present paper will compare this improved EOB approach to the *inspiralling* NR results of [20], we shall only make use here of the improvement (i).

A. Improved, resummed 3PN-accurate waveform

The new, resummed 3PN-accurate inspiral waveform[5] derived in Ref. [30] takes the form (when neglecting the "non quasi-circular" flexibility parameters, a and b, introduced to better represent the "plunge" which follows the inspiral)

$$\left(\frac{Rc^2}{GM}\right) h_{22}^{\text{inspiral}}(t) = -8\sqrt{\frac{\pi}{5}} \nu (r_\omega \Omega)^2 F_{22} e^{-2\mathrm{i}\Phi} , \quad (4)$$

where $\Phi(t)$ is the EOB orbital phase, $\Omega = \dot{\Phi}$ is the EOB orbital frequency, $r_\omega \equiv r\psi^{1/3}$ is a modified EOB radius [6],

---

in the comparable mass case $\nu \neq 0$.

[5] Contrary to Ref. [30] where we used a Zerilli-Moncrief normalized waveform Ψ_{22}, we use here the same h_{22} normalization as Ref. [41]. They differ simply by a numerical factor: $Rh_{\ell m} = \sqrt{(\ell+2)(\ell+1)\ell(\ell-1)} \left(\Psi_{\ell m}^{(e)} + \mathrm{i}\Psi_{\ell m}^{(o)} \right)$.

[6] The quantity r_ω is such that, during adiabatic inspiral, it is related to Ω by a standard Kepler-looking law $\Omega^2 r_\omega^3 = 1$, without correcting factors. However, during the plunge r_ω starts significantly deviating from $\Omega^{-2/3}$ [43].
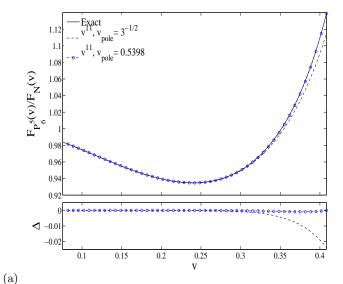

(a)

(b)

FIG. 1: Panel (a) compares the "exact" Newton-normalized flux function $\hat{F}(v)$ [39] to two different Padé resummed, v^{11}–accurate analytical flux functions: one using the standard value $v_{\text{pole}} = 1/\sqrt{3} = 0.57735$ and the other one using an "optimized" flexed value $v_{\text{pole}} = 0.5398$. The bottom part of (a) plots the corresponding differences $\Delta = \hat{F}^{\text{Pade}} - \hat{F}^{\text{Exact}}$. Panel (b) plots the same quantities, except for the fact that it uses only v^6–accurate analytical flux functions.

with ψ being defined in Eq. (22) of Ref. [43], and where the crucial novel PN-improving factor F_{22} is given as the product of four terms

$$F_{22}(t) = \hat{H}_{\text{eff}} T_{22} f_{22}(x(t)) e^{\mathrm{i}\delta_{22}(t)} . \quad (5)$$

Here $\hat{H}_{\text{eff}}$ is the *effective* EOB Hamiltonian divided by μ (it describes the quasi-geodesic dynamics of the "effective test mass" μ), and T_{22} is the particularization to $\ell =$

$m = 2$ of a resummed "tail correction factor" introduced in Ref. [30]. Its explicit expression (in the general, finite ν case) reads

$$T_{\ell m} = \frac{\Gamma(\ell + 1 - 2i\hat{\hat{k}})}{\Gamma(\ell + 1)} e^{\pi \hat{\hat{k}}} e^{2i\hat{\hat{k}} \log(2kr_0)} , \qquad (6)$$

where $\hat{\hat{k}} \equiv G H_{\rm real} m \Omega$ differs from $k = m\Omega$ by a rescaling involving the *real* (rather than *effective*) EOB Hamiltonian. This "tail factor" is the exact resummation of an infinite number of "leading logarithms" appearing in the perturbative multipolar-post-Minkowskian (MPM) expansion [44–48] of "tail effects" in the (ℓ, m) radiative moment. For instance, at the leading order in the monopole×multipole interaction the radiative quadrupole $U_{ij}(T_R)$ contains a tail integral [49]

$$2GI \int_0^\infty d\tau M_{ij}^{(4)}(T_R - \tau) \left[\log\left(\frac{\tau}{2r_0}\right) + \frac{11}{12} \right] , \qquad (7)$$

while at the next to leading order it contains a tail integral [50]

$$2G^2 I^2 \int_0^\infty d\tau M_{ij}^{(5)}(T_R - \tau) \left[\log^2\left(\frac{\tau}{2r_0}\right) + c_1 \log\left(\frac{\tau}{2r_0}\right) + c_0 \right] . \qquad (8)$$

[Here, I denotes the monopole of the source, i.e. $I = M_{\rm ADM} = H_{\rm real}$]. The factor $T_{\ell m}$ resums the infinite series of the contributions to $U_{\ell m}$ proportional to

$$G^n I^n \int_0^\infty d\tau M_{\ell m}^{(\ell + 1 + n)}(\tau_R - \tau) \log^n\left(\frac{\tau}{2r_0}\right) . \qquad (9)$$

The real factor $f_{22}(x)$ was computed in Ref. [30] (as indicated in footnote 8 there) to 3 PN accuracy for all values of ν by starting from the 3 PN-accurate multipolar post-Minkowskian results of Refs. [51–55]. The explicit form of its (PN) "Taylor" expansion reads

$$f_{22}^{\rm Taylor}(x) = 1 + \frac{1}{42}(-86 + 55\nu)x$$
$$+ \frac{1}{1512}\left(-4288 - 6745\nu + 2047\nu^2\right)x^2$$
$$+ \left(\frac{21428357}{727650} - \frac{856}{105}\text{eulerlog}(x) - \frac{34625}{3696}\nu\right.$$
$$+ \left.\frac{41}{96}\pi^2\nu - \frac{227875}{33264}\nu^2 + \frac{114635}{99792}\nu^3\right)x^3$$
$$+ \left(-\frac{5391582359}{198648450} + \frac{36808}{2205}\text{eulerlog}(x)\right)x^4$$
$$+ \left(-\frac{93684531406}{893918025} + \frac{458816}{19845}\text{eulerlog}(x)\right)x^5$$
$$+ \mathcal{O}(\nu x^4) + \mathcal{O}(x^6) . \qquad (10)$$

where $\text{eulerlog}(x) \equiv \gamma_{\rm E} + 2\log 2 + \frac{1}{2}\log x$. For greater accuracy, we have added in Eq. (10) the small ν limit of the 4PN and 5PN contributions (as deduced from the results of [40, 56]).

Finally, the additional phase $\delta_{22}(t)$ is given by

$$\delta_{22} = \frac{7}{3}H_{\rm real}\Omega + \frac{428}{105}\pi\left(H_{\rm real}\Omega\right)^2 - 24\nu x^{5/2} . \qquad (11)$$

At the time of the writing of [30] we had derived the full ν-dependent waveform (4)-(11), except for the accurate value of the coefficient of $\nu x^{5/2}$ in Eq. (11), because this value was not meaningful for us as it could be absorbed in the "non quasi-circular phase flexibility parameter" b included in Eq. (14) of [30]. Taking $b = 0$, we have recently derived from scratch the value -24 for this coefficient[7]. In the meantime, Kidder [41] has independently realized that it might be useful to compute the $\ell = m = 2$ part of the waveform to 3 PN accuracy and has derived a 3 PN-accurate non-resummed $(2, 2)$ waveform [See also [42] for an earlier 2.5 PN-accurate derivation of the (non-resummed) $(2, 2)$ waveform]. We have compared our result (5)-(11) with his and found perfect agreement (when PN-reexpanding our result).

Speaking of choices, there are more to be made to convert the PN-expanded amplitude factor $f_{22}^{\rm Taylor}$, Eq. (10), into a better, "resummed" EOB waveform factor. As said in Ref. [30], we propose to improve the convergence properties of the Taylor expansion (10) by replacing it by a suitable Padé approximant. We use the upper diagonal $(3, 2)$ Padé, i.e. we use in our calculations $f_{22}(x; \nu) = P_2^3\left[f_{22}^{\rm Taylor}(x; \nu)\right][8]$. The final choice we need to make concern the argument $x(t)$ of $f_{22}(x(t))$ in Eq. (10). As discussed in Ref. [30] this argument is "degenerate" during the inspiral in that it can be equivalently expressed in various ways in terms of the dynamical variables of the system, namely (in the general finite ν case) $x = \Omega^{2/3} = (r_\omega\Omega)^2 = 1/r_\omega$. We emphasized that some choices might be better than others to automatically capture some non quasi-circular effects during the plunge. However, as we are here concerned with the inspiral phase, we do not expect that the precise choice of $x(t)$ will matter. Some preliminary checks indicate that

---

[7] As was emphasized in Refs. [20, 41, 57] the small additional phase term $\propto \nu x^{5/2}$ has anyway very little effect on observable quantities during the inspiral.

[8] A technical remark concerning the Padé approximants we use (both for the flux function $F(v)$ and the waveform $f_{22}(x)$): contrary to the prescription suggested in Ref. [1], we find simpler (and numerically more or less equivalent) not to factor out the log-dependent terms (appearing at 3 PN and beyond), but instead to define the Padé approximants by considering the logarithms appearing in the PN expansion on par with the normal numerical Taylor coefficients: e.g., $1 + c_1 x + \cdots + (c_3^0 + c_3^1 \log x)x^3$ is Padéed by first Padeing the usual Taylor series $1 + c_1 x + \cdots + c_3 x^3$, and then replacing $c_3 \to c_3^0 + c_3^1 \log x$ in the result.

this is indeed the case. For simplicity, we shall use here the argument $x(t) = \Omega^{2/3}$ for $f_{22}(x(t))$ in Eq. (5).

B. Effective One Body relative dynamics

Let us briefly recall here the EOB construction of the relative dynamics of a two-body system (for more details on the recent improvements in the EOB approach see [28, 30]). The EOB approach to the general relativistic two-body dynamics is a *non-perturbatively resummed* analytic technique which has been developed in Refs. [2–5, 28, 30, 43]. The EOB approach uses as basic input the results of PN and MPM perturbation theory, and then "packages" this PN-expanded information in special *resummed* forms, which are expected to extend the validity of the PN results beyond their normal weak-field-slow-velocity regime into (part of) the strong-field-fast-motion regime. At the practical level, and for what concerns the part of the EOB approach which deals with the relative orbital dynamics, the method consists of two fundamental ingredients: (i) the "real Hamiltonian" $H_{\rm real}$, and (ii) the radiation reaction force $\mathcal{F}_\varphi$.

It is convenient to replace the adimensionalized radial momentum p_r (conjugate to the EOB adimensionalized radial coordinate $r = R/M$) by the conjugate p_{r_*} to the "EOB tortoise radial coordinate"

$$\frac{dr_*}{dr} = \left(\frac{B}{A}\right)^{1/2} ; \quad B \equiv \frac{D}{A} . \tag{12}$$

In terms of p_{r_*} (and after the rescaling $\hat{H}_{\rm eff} \equiv H_{\rm eff}/\mu$, $p_\varphi \equiv P_\varphi/(\mu M)$) the real, 3 PN-accurate Hamiltonian [4] reads

$$H_{\rm real}(r, p_{r_*}, p_\varphi) \equiv \mu \hat{H}_{\rm real} = M \sqrt{1 + 2\nu \left(\hat{H}_{\rm eff} - 1\right)} , \tag{13}$$

with

$$\hat{H}_{\rm eff}(r, p_{r_*}, p_\varphi) \equiv \sqrt{p_{r_*}^2 + A(r)\left(1 + \frac{p_\varphi^2}{r^2} + z_3 \frac{p_{r_*}^4}{r^2}\right)} , \tag{14}$$

where $z_3 = 2\nu\,(4 - 3\nu)$, and where the PN expansion of the crucial radial potential $A(r)$ $\left(\equiv -g_{00}^{\rm effective}\right)$ has the form [2, 4]

$$A^{\rm Taylor}(u) = 1 - 2u + 2\nu u^3$$
$$+ \left(\frac{94}{3} - \frac{41}{32}\pi^2\right)\nu u^4 + a_5 \nu u^5 + \mathcal{O}(\nu u^6) , \tag{15}$$

with $u = 1/r$. As suggested in Ref. [5] we have parametrized the presence of presently uncalculated 4 PN (and higher) contributions to $A(u)$ by adding a term $+a_5(\nu)u^5$, with the simple form $a_5(\nu) = a_5\nu$. [Indeed, it was remarkably found, both at the 1 PN, 2 PN [2],

and the 3 PN [4] levels, that, after surprising cancellations between higher powers of ν in the various contributions to the coefficient $a_n(\nu) = a_n^1 \nu + a_n^2 \nu^2 + \cdots$ of u^n in $A(u)$, only the term linear in ν remained for $n=2$,[9] 3 and 4. Ref. [5] introduced this term with the idea that "one might introduce a 4 PN contribution $+a_5(\nu)u^5$ to $A(u)$, as a free parameter in constructing a bank of templates, and wait until LIGO-VIRGO-GEO get high signal-to-noise ratio observations of massive coalescing binaries to determine its numerical value". We do not dispose yet of such real observations, but, as substitutes we can (as started in Refs. [22, 29]) try to use numerical simulations to determine (or at least constrain) the value of the unknown parameter a_5. This is what we shall do below, where we shall compare our results to previous ones.

As discussed in [4], the most robust choice[10] for resumming the Taylor-expanded function $A(u)$ is to replace it by the following Padé approximant $A(u) \equiv P_4^1[A^{\rm Taylor}(u)]$. Similarly, the secondary metric function $D(u) = P_3^0[D^{\rm Taylor}(u)]$ where $D^{\rm Taylor}(u)$ is given in Eq. (2.19) of Ref. [5].

The EOB equations of motion for $(r, r_*, p_{r_*}, \varphi, p_\varphi)$ are then explicitly given by Eqs. (6-11) of Ref. [28]. They are simply Hamilton's equations following from the Hamiltonian (13), except for the p_φ equation of motion which reads

$$\frac{dp_\varphi}{dt} = \hat{\mathcal{F}}_\varphi , \tag{16}$$

where, following Refs. [1, 3] the r.h.s. contains a *resummed* radiation reaction force, which we shall take in a form recently suggested in Ref. [43], namely

$$\hat{\mathcal{F}}_\varphi \equiv \frac{\mathcal{F}_\varphi}{\mu} = -\frac{32}{5}\nu\Omega^5 r_\omega^4 \frac{f_{\rm DIS}(v_\varphi; \nu, v_{\rm pole})}{1 - v_\varphi/v_{\rm pole}} , \tag{17}$$

where $v_\varphi \equiv \Omega r_\omega$, $r_\omega \equiv r\psi^{1/3}$ (with ψ defined as in Eq. (22) of Ref. [43]). Here $f_{\rm DIS}$ denotes a suitable Padé resummation of the quantity denoted $\hat{F}'^{\rm Taylor}(v, v_{\rm pole})$ above, i.e., the Taylor expansion of $(1 - v/v_{\rm pole})\hat{F}^{\rm Taylor}(v; \nu)$ where $\hat{F}^{\rm Taylor}$ is the Newton-normalized (energy or) angular momentum flux along circular orbits (expressed in terms of $v_{\rm circ} = \Omega^{1/3}$ for comparable-mass circular orbits). Here again, to completely define $\hat{\mathcal{F}}_\varphi$ we must clearly state what is the starting Taylor-expanded result that we use, and how we resum it. For greater accuracy, we are starting from

$$\hat{F}^{\rm Taylor}(v; \nu) = 1 + A_2(\nu)v^2 + A_3(\nu)v^3 + A_4(\nu)v^4$$
$$+ A_5(\nu)v^5 + A_6(\nu, \log v)v^6 + A_7(\nu)v^7$$
$$+ A_8(\nu = 0, \log v)v^8 , \tag{18}$$

---

[9] Actually, for $n = 2$, i.e. the 1 PN contribution to $A(u)$, the cancellations even led to a complete cancellation $a_2(\nu) = 0$!

[10] And the simplest one ensuring continuity with the $\nu \to 0$ limit.

where we have added to the known 3.5 PN-accurate [51–55] comparable-mass flux the small-mass-ratio 4 PN contribution [40]. Then, we use as Padé approximant of this (quasi-)v^8-accurate expansion $f_{\rm DIS}(v; v, v_{\rm pole}) \equiv P_4^4 \left[(1 - v/v_{\rm pole}) \hat{F}^{\rm Taylor}(v; \nu) \right]$. We indeed found that this specific (diagonal) Padé approximant (as well as the less accurate P_3^3 one) was robust under rather large variations of the numerical value of $v_{\rm pole}$ (by contrast to other ones, such as P_4^3 or P_3^4, which exhibit spurious poles when $v_{\rm pole}$ becomes too small). Finally, note that, for integrating the EOB dynamics from some finite starting radius (or frequency) we need some appropriate initial conditions. Refs. [3, 25, 58] indicated how to define some "post-adiabatic" initial conditions. In view of the high accuracy of the NR data of [20] (and notably of their extremely reduced eccentricity), we found useful to go beyond Refs. [3, 25, 58] and to define some, iterated "post-post-adiabatic" initial data allowing us to start integration at a radius $r = 15$.

Summarizing: In the comparable-mass case, the phasing, and the amplitude, of the new, resummed 3 PN-accurate inspiral waveform introduced in Ref [30] is given by inserting the solution of the EOB dynamics (given by Eqs. (13)-(17)) into the waveform (4)-(11). This waveform depends on two *flexibility parameters*, a_5 and $v_{\rm pole}$, that parametrize (in an effective manner) current uncertainties in the EOB approach: a_5 parametrizes uncalculated 4 PN and higher *orbital effects*, while $v_{\rm pole}$ parametrizes uncertainties in the *resummation of radiation effects* (also linked to ν dependent 4 PN and higher radiative effects).

IV. COMPARING THE NEW, RESUMMED EOB WAVEFORM TO ACCURATE NUMERICAL DATA

Thanks to the recent breakthroughs in numerical relativity one can now start to make detailed comparisons between EOB waveforms and numerical relativity ones. Working with high-accuracy data can further allow us to calibrate the "flexibility parameters" [25] entering extended versions of the EOB formalism. A first step in this direction was recently taken by Buonanno et al. [29] by utilizing numerical gravitational waveforms generated in the merger of comparable-mass binary black holes. However, the merger data that were used were relatively short (about 7 inspiralling orbits before merger when $\nu = 1/4$). Here, we shall instead consider the information contained in a recent, high accuracy, low-eccentricity simulation covering 15 orbits of an inspiralling equal-mass binary black hole [20]. [See also the previous results of the Jena group which covered ~ 9 inspiralling orbits [59]].

Boyle et al. [20] have published their results in the form of *differences* between the numerical relativity data and various, Taylor-type PN predictions We recall that there are many ways of defining some Taylor-type PN waveforms. Ref. [60] introduced a nomenclature which

included three sorts of PN-based "Taylor approximants"; from Taylor T1 to Taylor T3, as well as several other resummed approximants (Padé, and EOB). In addition, the definition of each such Taylor approximant makes two further choices: the choice of PN accuracy on the phasing, and the choice of PN accuracy in the amplitude. A fourth Taylor approximant, T4, was also considered in previous NR-PN comparison [26, 27, 61] and Ref. [26] had pointed out that it seemed to yield a phasing close to the NR one. Boyle et al. [20] confirmed this "experimental" fact and found that Taylor T4 at 3.5 PN phasing accuracy agreed much better with their long, accurate simulations than the other Taylor approximants.

Here we shall use as EOB quadrupolar metric waveform the new, resummed 3 PN-accurate inspiral waveform explicitly presented above, say $h_{22}^{\rm EOB}(t; a_5, v_{\rm pole})$, defined in Eq. (4) and the following equations of the previous section. Note, however, that [20] uses as basic gravitational radiation variable the $\ell = m = 2$ projection of the corresponding Weyl curvature quantity, which is related to the *metric* waveform h_{22} by

$$\left(\frac{Rc^2}{GM} \Psi_4^{22\rm X} \right)(t) \equiv \frac{\partial^2}{\partial t^2} \left(\frac{Rc^2}{GM} h_{22}^{\rm X} \right)(t) \equiv A_{\rm X}(t) e^{-{\rm i}\phi_{\rm X}(t)} . \tag{19}$$

Here, A and ϕ denote the *amplitude* and *phase* of the curvature wave considered by Boyle et al. [20]. We have introduced a label X which will take, for us, *three* values: X≡NR denotes the numerical relativity result of Ref. [20], X≡EOB denotes the improved EOB waveform presented in the previous section and X=T4 will denote the "Taylor T4" waveform highlighted in Ref. [20] (as well as in previous PN-NR comparisons [27, 61]) as giving a particularly good fit.

The precise definition of this T4 waveform (as used in Ref. [20]) is as follows. As indicated in Eq. (19), $\Psi_4^{22\rm T4}$ is obtained by taking two time derivatives of a corresponding metric T4 waveform $h_{22}^{\rm T4}$. The latter waveform is defined (if we understand correctly the combined statements of Refs. [20] and [41]) by the following procedure. First, one defines a certain "T4 orbital phase" $\Phi_{\rm T4}(t)$ by integrating the ODEs

$$\frac{d\Phi_{\rm T4}}{dt} = \frac{x^{3/2}}{GM} , \tag{20}$$

$$\frac{dx}{dt} = \frac{64\nu}{5GM} x^5 a_{3.5}^{\rm Taylor}(x) , \tag{21}$$

where

$$a_{3.5}^{\rm Taylor}(x) = 1 + \bar{a}_2(\nu)x + \bar{a}_3(\nu)x^{3/2} + \bar{a}_4(\nu)x^2 + \bar{a}_5(\nu)x^{5/2} + \bar{a}_6(\nu, \log x)x^3 + \bar{a}_7(\nu)x^{7/2} , \tag{22}$$

is the 3.5 PN Taylor approximant (for finite ν) to the Newton-normalized ratio (flux-function)/(derivative of energy function)=$F(v)/E'(v)$, which enters the adiabatic evolution of the orbital phase (see, e.g. [1, 60]). In the relevant case $\nu = 1/4$, $a_{3.5}^{\rm Taylor}(x)$ is explicitly given

as the quantity within curly braces on the r.h.s. of Eq. (45) of [20]. Having in hand the result, $\Phi_{T4}(t)$, $\Omega_{T4}(t) \equiv d\Phi_{T4}/dt \equiv x_{T4}^{3/2}/GM$, of integrating Eqs. (20)-(21) one then defines a nPN-accurate, T4 ($\ell = 2, m = 2$) waveform by truncating to order $x_{T4}^{n/2}$ included the Taylor series

$$\left(\frac{c^2 R}{GM} h_{22}^{T4}\right)(t) = -8\sqrt{\frac{\pi}{5}}\nu e^{-2i\Phi_{T4}(t)}x_{T4}$$

$$\times \left[1 + \tilde{h}_2 x_{T4} + \tilde{h}_3 x_{T4}^{3/2} + \tilde{h}_4 x_{T4}^2 + \tilde{h}_5 x_{T4}^{5/2} + \tilde{h}_6 x_{T4}^3\right],$$

(23)

where the coefficients $\tilde{h}_n$ are obtained from the coefficients h_n in the Taylor-expanded 3 PN-accurate (2,2) waveform derived by Kidder [41] by *setting to zero* all the terms proportional to $\log(x/x_0)$ or $\log^2(x/x_0)$ (but keeping the separate $\log x$ term entering h_6), and replacing $\nu = 1/4$.

Note that our resummed waveform (4)-(11) differs from the 3 PN-accurate version of (23) in several ways: (i) the "orbital phase" evolution is given, for us, by the EOB resummed dynamics, (ii) we do not neglect the phase terms linked to $\log(x/x_0)$, but include them either in the resummed tail factor T_{22} or in δ_{22}, and (iii) we resum the amplitude of h_{22} by factoring both $\hat{H}_{\text{eff}}$ and the modulus of T_{22}, and by Padeing f_{22}.

Ref. [20] presents in their Fig. 19 the differences, in phase and amplitude (of the radiative Weyl-curvature components Ψ_4), between Taylor T4 3.5/2.5 (i.e., 3.5 PN in phase and 2.5 PN in amplitude) and the (unpublished) corresponding Caltech-Cornell NR data, say

$$(\Delta\phi)_{T4NR} \equiv \phi_{T4}(t) - \phi_{NR}(t),$$ (24)

$$\left(\frac{\Delta A}{A}\right)_{T4NR} \equiv \frac{A_{T4}(t) - A_{NR}(t)}{A_{NR}(t)},$$ (25)

as plotted in the two panels of Fig. 19 of Ref. [20]. Our main aim here is to compare the "numerical data" (24)-(25) to the corresponding theoretical predictions made by the EOB formalism, say

$$(\Delta\phi)_{T4EOB} \equiv \phi_{T4}(t) - \phi_{EOB}(t),$$ (26)

$$\left(\frac{\Delta A}{A}\right)_{T4EOB} \equiv \frac{A_{T4}(t) - A_{EOB}(t)}{A_{EOB}(t)}.$$ (27)

As just said, as the most complete, and best plotted data, concern Taylor T4 3.5/2.5, we shall use the 3.5 PN accurate Eq. (22) but only consider the 2.5 PN truncation of the Taylor-expanded waveform (23) (i.e. a waveform essentially contained in the 2.5 PN h_+ and $h_\times$ results of Arun et al. [62]). [As we use the T4 waveform only as an *intermediary* between the NR and EOB results, we are allowed to use any convenient "go between", even if its PN accuracy differs from the (formal) one of our resummed EOB waveform].

To effect the comparison between NR and EOB, i.e., to compute the crucial difference $\phi_{EOB} - \phi_{NR}$, we needed to extract actual numerical data from Fig. 19 of [20]. We did that in several ways. First, we measured (with millimetric accuracy; on an A3-size version of the left panel of Fig. 19) sufficiently many points on the solid upper curve (Taylor T4 3.5/2.5 matched at $M\omega_4 = 0.1$) [11] to be able to replot (after "splining" our measured points) this upper curve with good (visual) accuracy. We could then use this splined version of eleven (adequately distributed) selected points on the upper curve on the left panel of Fig. 19 as our basic (approximate) "numerical data". It gives us a (continuous) approximation to the ω_4-matched phase difference $\Delta^{\omega_4}\phi_{T4NR}(\bar{t}^{\omega_4}) = \phi_{T4}^{\omega_4}(\bar{t}'_{T4}) - \phi_{NR}(\bar{t}^{\omega_4})$. [Here, $\bar{t}^{\omega_4}$ denotes the time shifted so that $\bar{t}^{\omega_4} = 0$ corresponds to the ω_4 matching point between T4 and NR]. As we have separately computed $\phi_{T4}(t_{T4})$ by integrating Eqs. (20)-(21) (and that it is easy to shift it to obtain $\phi_{T4}^{\omega_4}(\bar{t}'_{T4})$) we have thereby obtained an approximation to $\phi_{NR}(\bar{t}^{\omega_4})$. We then shift again the time argument to our basic EOB dynamical time so as to obtain $\phi_{NR}(t_{EOB})$ (with the condition that $\omega_{EOB}(t_{EOB}^{\omega_4}) = \omega_4$ corresponds to $\bar{t}^{\omega_4} = 0$).

There are then several ways of comparing $\phi_{NR}(t_{EOB})$ to the EOB phasing $\phi_{EOB}(t_{EOB})$, obtained from the procedure explicated above. We wish to emphasize here that there is a useful way of dealing with the information contained in (any) phasing function $\phi_X(t_X)$ where X=NR, EOB, T4, etc. Indeed, a technical problem concerning any such phasing function is the presence of two shift ambiguities: a possible arbitrary shift in ϕ_X ($\phi_X \to \phi_X + c_X$) and a possible arbitrary shift in the time variable t_X ($t_X \to t_X + \tau_X$). Similarly to what one does in Euclidean plane geometry where one can replace the Cartesian equation of a curve $y = y(x)$ by its *intrinsic* equation $K = K(s)$ (where K is the curvature and s the proper length), we can here (in presence of a different symmetry group) replace the shift-dependent phasing function $\phi_X(t_X)$ by the shift-independent *intrinsic* phase evolution equation: $d\omega_X/dt_X = \alpha_X(\omega_X)$, where $\omega_X \equiv d\phi_X/dt_X$ (for simplicity we shall use here $M = m_1 + m_2 = 1$). It is also convenient to factor out of the *phase acceleration* $\alpha_X(\omega)$ its "Newton" approximation [12],

$$\alpha_N(\omega) \equiv c_\nu \omega^{11/3}; \qquad c_\nu = \frac{12}{5}2^{1/3}\nu \qquad (28)$$

and to consider the reduced phase acceleration function

---

[11] Ref. [20] computes various differences $\Delta^{\omega_m}\phi(t) = \phi_{T4}^{\omega_m}(t'_{T4}) - \phi_{NR}(t)$ where, given a "matching" frequency ω_m, $\phi_{T4}^{\omega_m}(t'_{T4})$ denotes a version of $\phi_{T4}(t_{T4})$ which is shifted in ϕ and in t so that $0 = \Delta^{\omega_m}\phi(t) = d\Delta^{\omega_m}\phi(t)/dt$ at the moment $t_{NR}^{\omega_m}$ where $d\phi_{NR}/dt = \omega_m$. We shall denote the four matching frequencies used in [20] as $M\omega_1 \equiv 0.04$, $M\omega_2 = 0.05$, $M\omega_3 = 0.063$, $M\omega_4 = 0.1$

[12] Note that we are dealing here with the gravitational (curvature) wave frequency ω. If we were dealing with the orbital frequency $\Omega = d\Phi/dt$, we would instead consider the following reduced phase acceleration $(d\Omega/dt)/(C_\nu \Omega^{11/3}) = A_\Omega(\Omega)$ with $C_\nu = (96/5)\nu$.
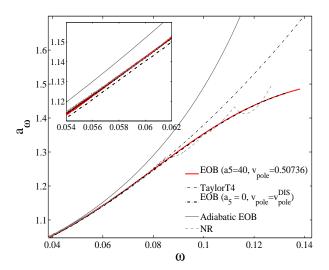
FIG. 2: Reduced phase-acceleration curves as defined in Eq. (29) (with $M \equiv m_1 + m_2 = 1$). The inset highlights how the "tuned" EOB curve nearly coincides (for $\omega \lesssim 0.08$) with the NR (and T4) curves, while the "non-tuned" EOB one lies slightly below.

a_ω^{X} defined by

$$\frac{\dot{\omega}_{\mathrm{X}}}{c_\nu \omega_{\mathrm{X}}^{11/3}} = a_\omega^{\mathrm{X}}(\omega_{\mathrm{X}}) \, . \tag{29}$$

Independently of the label X the function $a_\omega^{\mathrm{X}} \to 1$ as $\omega \to 0$. The phasing comparisons then boil down to comparing the various (reduced) phase acceleration functions $a_\omega^{NR}(\omega)$, $a_\omega^{T4}(\omega)$ and $a_\omega^{\mathrm{EOB}}(\omega; a_5, v_{\mathrm{pole}})$. The last two functions can be straightforwardly (numerically) computed from the formulas written above. As for $a_\omega^{NR}(\omega)$ it is, in principle, also straightfiorwardly computable from $\phi_{\mathrm{NR}}(t_{\mathrm{NR}})$. However, as we do not have access to an accurate estimate of $\phi_{\mathrm{NR}}(t_{\mathrm{NR}})$ but only to a rather rough cubic spline approximation to it, we can only compute an even rougher estimate of $a_\omega^{NR}(\omega)$. [As is well known, taking (two!) derivatives of approximate results considerably degrades the accuracy.] Still, as we think that this is the conceptually clearest way of presenting the comparison, we used the data we had in hand to compute the various "acceleration curves" presented in Fig. 2.

Actually, it is instructive to include further phase-accelerations in the comparison. In Fig. 2 we show the following phase-acceleration functions (versus ω, i.e., $M\omega$): (i) Taylor T4 3.5/2.5, (ii) NR, (iii) a standard "non-tuned" EOB with $a_5 = 0$ (i.e. essentially the 3 PN approximation) and $v_{\mathrm{pole}} = v_{\mathrm{pole}}^{\mathrm{DIS}}(\nu)$ [1] for $\nu = 1/4$, which corresponds to our current knowledge, (iv) a "tuned" EOB with $a_5 = 40$ and $v_{\mathrm{pole}} = 0.5074$ (see below), and finally (v) the *adiabatic* EOB for $a_5 = 40$ and $v_{\mathrm{pole}} = 0.5074$. Here, the *adiabatic* approximation to a_ω is that defined by the usual adiabatic approach

to inspiral phasing (see e.g. [1]), leading to $a_\omega(\omega) = \hat{F}(v)/\hat{E}'(v)$ where $v = (\omega/2)^{1/3}$ and where $\hat{F}$ is the Newton-normalized circular flux and $\hat{E}'$ the Newton-normalized derivative of the circular energy function. [When applying these general concepts to the EOB we need, as discussed in Ref. [3], to use the analytical, adiabatic approximation to EOB inspiral, with, notably, $p_\varphi = j^{\mathrm{adiabatic}}(u)$ obtained by solving $\partial H_{\mathrm{EOB}}/\partial r = 0$ with $p_r = 0$].

Several preliminary conclusions can be read off Fig. 2.

(i) In the frequency domain (say $M\omega < 0.08$) where the T4 3.5 phasing matches well with the NR phasing, both the standard "non-tuned" EOB ($a_5 = 0$, $v_{\mathrm{pole}} = v_{\mathrm{pole}}^{\mathrm{DIS}}$) and "tuned" EOB phasing (defined above) match well with the NR phasing. However, a closer look at the acceleration curves (see inset) shows that the "tuned" EOB phasing agrees better with NR (and T4). [The "non-tuned" a_ω^{EOB} is slightly below a_ω^{NR} (and a_ω^{T4}) by roughly 1.5×10^{-3} when $M\omega \sim 0.06$].

(ii) For higher frequencies ($0.08 < M\omega \lesssim 0.14$), Taylor T4 3.5/2.5 starts to significantly diverge from the NR phasing. [13] By contrast, both the standard "non-tuned" EOB phasing and the "tuned" EOB one continue to match quite well the NR phasing. This will be shown below by using other diagnostics than the acceleration curves. Indeed, when $M\omega \gtrsim 0.08$ our "NR acceleration curve" exhibits fake oscillations which come from our use of a coarse approximation to NR data. The visible "kinks" in our NR acceleration curve are due to our taking (numerical) second derivative of a *cubic spline* interpolant of *approximate* NR data points. We expect that the exact "NR acceleration curve" (computed with accurate numerical data instead of our approximate ones) will be a smooth curve lying close to the two EOB curves in Fig. 2.

(iii) The fact that the *adiabatic* EOB curve diverges quite early, and upwards, from the full EOB curve is a confirmation of the conclusion derived in Ref. [3] (see Figs. 4 and 5 there), namely that , " in the equal mass case $\nu = 1/4$ the adiabatic approximation starts to significantly deviate from the exact evolution quite before one reaches the LSO". This further confirms the suggestion of [20] that the good early ($M\omega < 0.08$) agreement between T4 and NR is coincidental.

Because of our lack of an accurate knowledge of a_ω^{NR}, we cannot use the acceleration curves of Fig. 2 to make any accurate comparison between EOB and NR data. In the following we shall use other tools for doing this comparison and, in particular, for constraining the values of a_5 and v_{pole}.

---

[13] Though Ref. [20] tends to mainly emphasize how well Taylor T4 3.5/2.5 agrees with the NR phasing one should note that the high curvature of the upper ω_4 curves when $M\omega \gtrsim 0.08$ in the left panel of Fig. 19, and the subsequent fast rise of all the $\Delta^{\omega m}\phi$, are clear signals that Taylor T4 3.5/2.5 starts to significantly (*and increasingly*) diverge from the NR phasing.
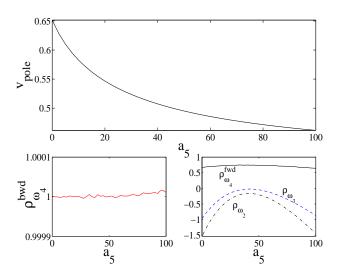
FIG. 3: Correlation between $v_{\rm pole}$ and a_5 (top panel) obtained by imposing the constraint (35). The numerical accuracy with which Eq. (35) is satisfied is displayed in the left-bottom panel. The right-bottom panel displays the extent to which, as a_5 varies, the other ratios ρ_{ω_m}, Eq. (34), approximate unity.

The first tool we shall use consists in selecting among our eleven approximate points on the $\Delta^{\omega_4}\phi_{\rm T4NR}$ curve two special ones, namely

$$\Delta^{\omega_4}\phi_{\rm T4NR}(t_{\rm NR}^{\omega_4} - 1809M) \equiv \delta_4^{\rm bwd} \simeq 0.055 \ , \qquad (30)$$

$$\Delta^{\omega_4}\phi_{\rm T4NR}(t_{\rm NR}^{\omega_4} + 44.12M) \equiv \delta_4^{\rm fwd} \simeq 0.01 \ , \qquad (31)$$

to which we shall refer as the (main) "backward" and "forward" ω_4 data. In addition, we also measured a couple of selected points on the ω_2- and ω_3-matched lower $\Delta\phi$ curves. Namely,

$$\Delta^{\omega_2}\phi(t_{\rm NR}^{\omega_2} + 1000M) \equiv \delta_2 \simeq -0.01 \ , \qquad (32)$$

$$\Delta^{\omega_3}\phi(t_{\rm NR}^{\omega_3} - 1000M \equiv \delta_3 \simeq -4.3 \times 10^{-3} \ . \qquad (33)$$

We can then use, in a numerically convenient way, these data to quantitatively compare (with an hopefully reasonable numerical accuracy) NR to EOB by considering four *ratios*, ρ_{ω_2}, ρ_{ω_3}, $\rho_{\omega_4}^{\rm bwd}$, $\rho_{\omega_4}^{\rm fwd}$ (where we recall that $\omega_2 = 0.05$, $\omega_3 = 0.063$ and $\omega_4 = 0.1$), with

$$\rho_{\omega_m}(a_5, v_{\rm pole}) \equiv \frac{\Delta^{\omega_m}\phi_{\rm T4EOB}(t_{\rm NR}^{\omega_m} + \delta t_m)}{\delta_m} \ , \qquad (34)$$

and $\omega_m = \omega_2$, ω_3 and $\omega_4^{\rm bwd}$ or $\omega_4^{\rm fwd}$.

If our approximate measures (given in Eqs. (30)-(33)) of the various δ_m's were accurate, a perfect match between NR and EOB would correspond to having all those ratios equal to unity: $\rho_{\omega_2}(a_5, v_{\rm pole}) = 1$, $\rho_{\omega_3}(a_5, v_{\rm pole}) = 1$, $\rho_{\omega_4}^{\rm bwd}(a_5, v_{\rm pole}) = 1$, and $\rho_{\omega_4}^{\rm fwd}(a_5, v_{\rm pole}) = 1$. This would give four equations
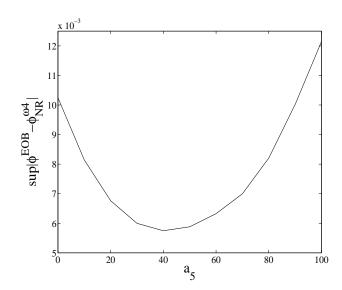

FIG. 4: The L_∞ norm of the phase difference between EOB (when $v_{\rm pole}$ is correlated to a_5 as in Fig. 3) and numerical relativity, as defined by Eq. (36).

for two unknowns (a_5 and $v_{\rm pole}$). Even if we had exact values for the various δ_m's, we do not, however, expect that there would exist special values of a_5 and $v_{\rm pole}$ for which *all* these ratios would be equal to one. Indeed, a_5 and $v_{\rm pole}$ are only "effective" parameters that are intended to approximately mimic an infinite number of higher ν-dependent, resummed PN-effects. The best we can hope for is to find values of a_5 and $v_{\rm pole}$ allowing one to give a good overall match between $\phi_{\rm NR}(t)$ and $\phi_{\rm EOB}(t)$ (or $a_\omega^{\rm NR}$ and $a_\omega^{\rm EOB}$). To investigate this issue, it is then convenient to focus first on only *one* comparison observable. We choose $\rho_{\omega_4}^{\rm bwd}$ because it is, among the data which we could measure with reasonable accuracy, the one which has the largest "lever arm". [Indeed, it corresponds to some weighted integral of the difference $a_\omega^{\rm EOB} - a_\omega^{\rm NR}$ over a significantly extended frequency interval]. Imposing the constraint

$$\rho_{\omega_4}^{\rm bwd}(a_5, v_{\rm pole}) = 1 \ , \qquad (35)$$

then gives a precise way of exploring which extended EOB models best match the NR phasing . Note first that this equation could have no solutions. [For instance, if we were using the *adiabatic* approximation to EOB there would be no solutions]. To admit solutions is already a sign that EOB can provide a much better match to NR than T4. Then, the solutions could exist only if both a_5 and $v_{\rm pole}$ are close to some "preferred" values. Actually, we found that Eq. (35) defines a *continuous curve* in the $(a_5, v_{\rm pole})$ plane[14].

---

[14] Consistently with what was found for lower approximations, and

For all values of $a_5 \geq 0$, we (numerically) found a unique value of v_{pole} satisfying the constraint (35). This continuous curve is plotted in the upper panel of Fig. 3. When remembering that Eq. (30) is only approximate,[15] we have to mentally replace the continuous curve in the upper panel of Fig. 3 by a narrow valley of "best fitting" values of (a_5, v_{pole}). Let us first remark that this valley extends only on a rather small range of values of v_{pole}, around 0.55. It is comforting that this range includes the values that were previously suggested for v_{pole}: namely $v_{\text{pole}}^{\text{usual}}(\nu = 0) = 1/\sqrt{3} = 0.57735$, $v_{\text{pole}}^{\text{DIS}}(\nu = 1/4) \simeq 0.6907$, $v_{\text{pole}}^{\text{best}}(\nu = 0) \simeq 0.54$ (discussed above).

To go beyond this result and see whether the other measurements constrain the value of a_5, we plot on the lower, right panel of Fig. 3 the values of the ratios ρ_{ω_2}, ρ_{ω_3} and $\rho_{\omega_4}^{\text{fwd}}$ *along* the $\rho_{\omega_4}^{\text{bwd}} = 1$ curve. As, along this curve, v_{pole} is a function of a_5, the above three ratios depend only on a_5. Ideally, we would like to find values of a_5 for which the remaining ratios are all close to unity. [Given the coarse nature of our measurements, we cannot expect to get exactly unity]. We see on Fig. 3 that the ratio $\rho_{\omega_4}^{\text{fwd}}$ is reasonably close to unity for most values of a_5. By contrast, the two other ratios ρ_{ω_2} and ρ_{ω_3} happen to have the *wrong sign*. This negative sign means, in terms of the phase-acceleration curves of Fig. 2, that around frequencies ω_2 and ω_3, $a_\omega^{\text{NR}}(\omega)$ is slightly *above* $a_\omega^{\text{T4}}(\omega)$, while it seems that $a_\omega^{\text{EOB}}(\omega)$ tends to be generally slightly *below* $a_\omega^{\text{T4}}(\omega)$. On the other hand, for larger frequencies, it seems clear that a_ω^{NR} crosses a_ω^{T4} to become *below* a_ω^{T4}, and to become in rather good agreement with a_ω^{EOB}. At this stage, the best we can do is to say that an overall best match between EOB and NR will be obtained when a_5 belongs to a rather large interval (say $10 \lesssim a_5 \lesssim 80$) centered around $a_5 \simeq 40$, where ρ_{ω_2} and ρ_{ω_3} are negative, but rather small (say $-0.5 \lesssim \rho_{\omega_3} \lesssim 0$)

To get another, potentially better measure of the "closeness" between NR and EOB we looked at the "L_∞" distance between the two functions $\phi_{\text{NR}}(t)$ and $\phi_{\text{EOB}}(t)$ on the time interval (in EOB time) $900M \leq t_{\text{EOB}} \leq 3460M$ (which roughly corresponds to the time interval plotted in Fig. 19 of Ref. [20]). More precisely, we computed the quantity

$$L_\infty(a_5) \equiv \sup_{900M \leq t_{\text{EOB}} \leq 3460M} \left| \phi_{\text{EOB}}(t_{\text{EOB}}) - \phi_{\text{NR}}^{\omega_4}\left(t'^{\omega_4}_{\text{NR}}\right) \right|,$$
(36)

where $\phi_{\text{NR}}^{\omega_4}\left(t'^{\omega_4}_{\text{NR}}\right)$ is matched to the EOB phase at ω_4, and where the EOB was constrained to lie along the curve $v_{\text{pole}}(a_5)$ plotted in Fig. 3 (i.e., satisfying Eq. (35)).
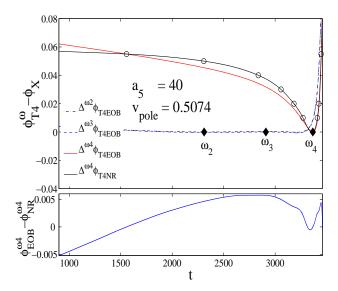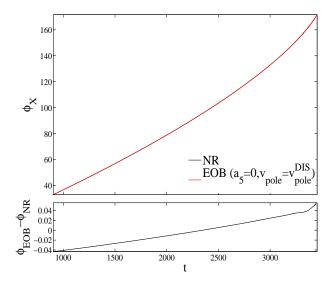
---

for the presently computable contributions to a_5 [25], we expect that $a_5 \geq 0$, and we shall therefore only work in the corresponding half plane.

[15] We estimate the accuracy of our measurement result Eq. (30) to be such that the "backward time-shift", corresponding to a r.h.s. exactly equal to 0.055, is $(-1809 \pm 15)M$.

FIG. 5: The upper panel compares various phase differences $\Delta^{\omega_m}\phi_{\text{T4X}}$ versus time (with $M = 1$), ω_m denoting a matching frequency and the label X being either EOB or NR. The lower panel exhibits the ω_4–matched phase difference between EOB and NR. The flexibility parameters of EOB have been tuned here to $a_5 = 40$ and $v_{\text{pole}} = 0.5074$.
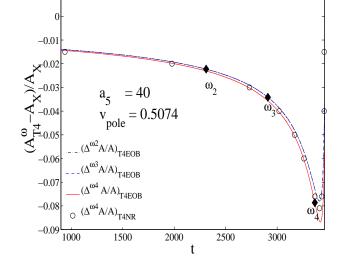
We show this L_∞ norm in Fig. 4. This Figure displays the remarkable agreement between EOB and NR phasing over an interval where T4 exhibits a clear dephasing with respect to NR. Indeed, Fig. 19 of [20] shows that on this interval all Taylor T4 3.5 templates dephase by ≈ 0.08 radians (because of the divergence at the end, corresponding to the divergence of the acceleration curves in Fig. 2 when $\omega \gtrsim 0.08$). By contrast, the dephasing between EOB and NR can be as small as 0.006 radians if $30 \lesssim a_5 \lesssim 52$, or 0.008 radians if $10 \lesssim a_5 \lesssim 80$. Again, we find that a largish interval of a_5 values centered around $a_5 \sim 40$ seems to be preferred (when v_{pole} is correlated to a_5 via the curve of Fig. 3) to give the best possible overall match between EOB and NR.

To give a better feeling of how well EOB matches NR phasing all over the time interval explored by the simulation of Ref. [20], we plot in Fig. 5 the superposition of the upper curve in Fig. 19 of [20] (i.e., the difference $\Delta^{\omega_4}\phi_{\text{T4NR}}$, as measured and splined by us) with the corresponding EOB difference $\Delta^{\omega_3}\phi_{\text{T4EOB}}$, for the values $a_5 = 40$, $v_{\text{pole}} = 0.5074$ approximately corresponding to the smallest L_∞ norm in Fig. 4. We also plot the ω_2- and ω_3-matched phase differences $\Delta^{\omega_2}\phi_{\text{T4EOB}}$ and $\Delta^{\omega_3}\phi_{\text{T4EOB}}$. Apart from the slightly wrong curvatures of the ω_2- and ω_3- curves (for $\omega \lesssim 0.08$), this Figure exhibits a truly remarkable visual agreement with the left panel of Fig. 19 of [20]. It exhibits again two facts: (i) the EOB phasing agrees extremely well with the NR one on the full time interval ($900M \leq t_{\text{EOB}} \leq 3460M$), (ii) by contrast Taylor T4 3.5/2.5 starts diverging from EOB

FIG. 6: Comparison between the standard, "non-tuned" EOB ($a_5 = 0$, $v_{\rm pole} = v_{\rm pole}^{\rm DIS}(\nu = 1/4) = 0.6907$) and NR. The top panel shows that the gravitational wave phases $\phi_{\rm EOB}$ and $\phi_{\rm NR}$ (versus time) are nearly indistinguishable to the naked eye. The bottom panel quantifies the small difference between the two.

FIG. 7: Comparison between relative amplitude differences $(\Delta^{\omega_m}A/A)_{\rm T4X}$ versus time, ω_m denoting the matching frequency and the label X being either EOB (for $a_5 = 40$, $v_{\rm pole} = 0.5074$) or NR.

when $\omega \gtrsim 0.08$ in precisely the same way that it diverges from NR. In the bottom panel of Fig. 5 we give a precise quantitative measure of the difference between EOB and NR phasings by plotting the ω_4-matched difference $\phi_{\rm EOB}(t) - \phi_{\rm NR}^{\omega_4}(t'_{\omega_4})$. This phase difference vanishes both when $\omega_{\rm EOB}(t_{\rm EOB}^{\omega_4}) = \omega_4$ (by construction), and at the time $t_{\rm EOB}^{\rm bwd} = t_{\rm EOB}^{\omega_4} - 1809M$ (by our optimized choice of the link $v_{\rm pole} = v_{\rm pole}(a_5)$, such that Eq. (35) holds). We see how, indeed (in agreement with Fig. 4) the dephasing remains smaller, in absolute value, than about 0.006 radians, i.e. 0.001 GW cycles.

This remarkably small dephasing concerns a "tuned" EOB phasing (with optimized flexibility parameters a_5 and $v_{\rm pole}$). However, as it is clear on Fig. 2, even the standard , "non-tuned" EOB phasing corresponding to our current analytical knowledge $a_5 = 0$, $v_{\rm pole} = v_{\rm pole}^{\rm DIS}(\nu)$, agrees quite well with the NR phasing over the entire simulation time. To exhibit this important fact in quantitative detail we compare in Fig. 6 the (splined) NR phase $\phi_{\rm NR}(t')$ (after suitable shifts in ϕ and t) to the standard, "non-tuned" EOB phase $\phi_{\rm EOB}(t)$ ($a_5 = 0$, $v_{\rm pole} = v_{\rm pole}^{\rm DIS}(\nu)$). As the *visual* agreement (top panel) is too good to allow one to distinguish the two curves, we show (bottom panel) the phase difference $\phi_{\rm EOB}(t) - \phi_{\rm NR}(t')$. As expected, the dephasing is less good than in the above "tuned" case, but it remains impressively good: ± 0.05 radians, i.e., ± 0.008 GW cycles, over the full time interval $900M \leq t_{\rm EOB} \leq 3460M$.

Finally, we claim that, not only the *phase*, but also the *amplitude* of the new, resummed EOB waveform

Eq. (4) exhibits a remarkable agreement with the NR data of [20]. Again, as Ref. [20] gave their results in the form of differences T4-NR, we plot in Fig. 7 the analog of the right panel of Fig. 19 there. We choose again the "optimum" values $a_5 = 40$, $v_{\rm pole} = 0.5074$ used in Fig. 5 and plot the NR → EOB analogs of the curves plotted by them in Fig. 19. Namely, we plot, at once, the ω_2-, ω_3- and ω_4-matched amplitude differences $[\Delta^{\omega_n}A/A]_{\rm T4EOB} = (A_{\rm T4}^{\omega_m} - A_{\rm EOB})/A_{\rm EOB}$, where, as above, the T4 time is shifted so that $\omega_{\rm T4}(t')$ and $\omega_{\rm EOB}(t)$ agree when $\omega_{\rm EOB}(t_m) = \omega_m$. In addition, we plot, as empty circles, some points taken (by approximate measurements of ours) from the corresponding curve $[\Delta^{\omega_4}A/A]_{\rm T4NR}$ plotted on the right panel of Fig. 19 of [20]. The remarkable visual agreement between these empty circles and our $(\Delta^{\omega_4}A/A)_{\rm T4EOB}$ curve shows that: (i) the new, resummed 3 PN amplitude introduced in Ref. [30] and defined in Eqs. (4) (11) above agrees remarkably well with the NR one on the full time interval, $900M \leq t_{\rm EOB} \leq 3460M$, (ii) by contrast the Taylor T4 3.5/2.5 PN amplitude shows a significant disagreement ($\sim -8\%$) in the same interval. Note that, though Ref. [20] emphasizes that the *non-resummed* 3 PN-accurate waveform of [41] "improves agreement significantly" compared to the 2.5 PN one (used above), this improvement only concerns the early part of the inspiral. Indeed, Fig. 21 of [20] shows that the amplitude of Taylor T4 3.5/3.0 tends again to diverge together with Taylor T4 3.5/2.5 at the end of the inspiral: i.e., we think, precisely around the "dip" (near ω_4) exhibited in Fig. 7 above.

V. CONCLUSIONS

We have investigated the agreement (in phase and in amplitude) between the predictions of the Effective-One-Body (EOB) formalism and some accurate numerical data. We used as numerical data both (as a warm up) some old results on the energy flux from circular orbits of a test mass around a non spinning black hole [39], and some very recent results of the Caltech-Cornell group about the $\ell = m = 2$ gravitational wave emitted by 15 orbits of an inspiralling system of two equal-mass non-spinning black holes [20].

In our warm up, test-mass example we showed how a slight tuning of the *flexibility parameter* [25] $v_{\rm pole}$ (away from the naively expected value $v_{\rm pole}^{\rm standard}(\nu = 0) = 1/\sqrt{3} = 0.57735$) to the value $v_{\rm pole}^{\rm best}(\nu = 0) \simeq 0.540$ allowed one to fit remarkably well the flux function $F(v; \nu = 0)$ during the full inspiral, $0 \le v \le v_{\rm LSO} = 1/\sqrt{6}$.

In the comparable mass case ($\nu = m_1 m_2/(m_1 + m_2)^2 \sim 1/4$) we followed [30] in introducing a new, resummed 3 PN-accurate[16] EOB-type $\ell = m = 2$ waveform. We then showed how to compute, for any values of the EOB flexibility parameters a_5 (parametrizing 4 PN and higher conservative orbital interactions) and $v_{\rm pole}$ (parametrizing ν-dependent 4 PN and higher effects in the resummed radiation reaction) the EOB predictions for the $\ell = m = 2$ gravitational curvature wave $\Psi_4^{22} \propto \partial_t^2 h_{22}^{\rm EOB} \propto A_{\rm EOB}(t) e^{-i\phi_{\rm EOB}(t)}$.

We then compared the EOB predictions for the gravitational wave (GW) phase, $\phi_{\rm EOB}(t)$, and amplitude, $A_{\rm EOB}(t)$, to the numerical relativity results of [20], say $\phi_{\rm NR}(t)$, $A_{\rm NR}(t)$, using often as intermediary (as Ref. [20]) the so-called Taylor T4 3.5/2.5 post-Newtonian predictions $\phi_{\rm T4}(t)$, $A_{\rm T4}(t)$. Our main conclusions are:

(i) In the GW frequency domain $M\omega < 0.08$ where the Taylor T4 3.5/2.5 phase matches well with the NR phase, the EOB phase matches at least as well with the NR phase. A good EOB/NR match is obtained both for the standard "non-tuned" EOB flexibility parameters $a_5 = 0$, $v_{\rm pole} = v_{\rm pole}^{\rm DIS}(\nu)$ corresponding to our current *analytical* knowledge [1, 4] and for "tuned" EOB flexibility parameters.

(ii) For higher GW frequencies, $0.08 < M\omega \lesssim 0.14$, while Taylor T4 3.5/2.5 starts to significantly diverge from the NR phase, we showed that the standard "non-tuned" EOB phasing continues to stay in phase with NR within $\pm 8 \times 10^{-3}$ GW cycles (see Fig. 6). Moreover, one can calibrate a_5 and $v_{\rm pole}$ so that the EOB phase matches with the NR phasing to the truly remarkable level of $\pm 10^{-3}$ GW cycles over 30 GW cycles!

(iii) We proposed several ways of "best fitting" the ($a_5, v_{\rm pole}$)-dependent EOB predictions to accurate NR data: (a) by using the *intrinsic* representation of the phase evolution given by the reduced phase-acceleration function $a_\omega(\omega)$, Eq. (29); (b) by using selected ratios $\Delta^{\omega_m}\phi_{\rm T4EOB}/\Delta^{\omega_m}\phi_{\rm T4NR}$ and constraining them to be close to unity; and (c) by using an L_∞ norm of the difference between (ω_m-matched) $\phi_{\rm EOB}(t)$ and $\phi_{\rm NR}^{\omega_m}(t'_{\omega_m})$.

Our results are given in several Figures. Notably, Fig. 3 gives, for each given value of a_5, what is the optimum value of $v_{\rm pole}$ which best fits (in the sense of the ratio $\rho_{\omega_4}^{\rm bwd}$, Eq. (35)) the NR data. Then, Fig. 4 plots the L_∞ distance (on a large time-interval roughly corresponding to the full simulation of [20]) between $\phi_{\rm EOB}(t)$ and $\phi_{\rm NR}^{\omega_4}(t'_{\omega_4})$ as a function of a_5 (for $v_{\rm pole} = v_{\rm pole}(a_5)$ given by Fig. 3). We find that the absolute value of the maximum dephasing between EOB and NR can be as small as 0.006 radians (or 0.001 GW cycles) if $30 \lesssim a_5 \lesssim 52$. However, it is difficult to be precise about the "preferred" valued of a_5. We recall in this respect that, recently, Ref. [29] has tried to constrain the value of a_5 (keeping, however, $v_{\rm pole}$ fixed to $v_{\rm pole}^{\rm DIS}(\nu)$, and without using our improved EOB waveform) by maximizing the overlap between EOB and NR plunge waveforms. They found that the overlap was good (and flat) over a rather large interval of values of a_5 (that they denote as λ), roughly centered around $a_5 \simeq 60$. We note, however, that this behavior might be due (at least in part) to the phenomenon pointed out in [25]. In the latter reference (where a_5 was denoted as b_5), it was found that the use of EOB templates based on $a_5 = 50$ (rather than $a_5 = 0$) allowed one to have large overlaps (large "effectualnesses") with all other EOB templates. At this stage, we therefore do not have yet any precise knowledge of what might be the preferred "effective" value of a_5. Our work, however, shows that there is a quite strict correlation between the best-fit choices of a_5 and $v_{\rm pole}$. When, in the future, a_5 becomes precisely known, it will be interesting to see what is the corresponding value of $v_{\rm pole}(\nu = 1/4)$ and to compare it to the best-fit value $v_{\rm pole}(\nu = 0) \simeq 0.540$ obtained in our warm-up Sec. II.

For instance, the couple $a_5 = 40$, $v_{\rm pole} = 0.5074$ yields a remarkable good fit to the NR data reported in [20]. We show the comparison of the various phasings (NR, EOB, T4) in Fig. 5. This Figure clearly exhibits how our best-fit EOB phase does a much better job than any non-resummed PN approximant at following the NR phase. We finally get dephasings smaller than ± 0.006 radians (i.e. $< 10^{-3}$ GW cycles!) over about 30 GW cycles!

Finally, we exhibited in Fig. 7 how the amplitude of our new, resummed 3^{+2}-PN-accurate EOB waveform, Eq. (4), exhibits a remarkable agreement with the corresponding amplitude of the NR data of [20]. The agreement is clearly better than any, non resummed PN amplitude, including the recent 3 PN-accurate one of Kidder [41].

We think that the present work, taken in conjunction with other recent works on the EOB-NR compar-

---

[16] Actually, our waveform has a greater accuracy than 3 PN in that it incorporates the test-mass limit of the 4 PN and 5 PN amplitude corrections. We shall occasionally refer to this PN accuracy as being 3^{+2}-PN.

ison [29] [28, 30], confirms the remarkable ability of the EOB formalism (especially in its recently improved avatars) to agree with NR results. Note in particular that the level of phase agreement reached here is better by a factor 30 (± 0.001 GW cycles versus ± 0.03 GW cycles for $\nu = 1/4$) than what was recently achieved, for merger signals, in Ref. [29] using less accurate versions of EOB waveforms than the one used here. We suggest that the ground-based interferometric GW detectors should include in their template banks the new, extended and improved EOB waveforms which are being developed and notably the resummed one introduced in [30] and generalized here. We also suggest that NR data be made available in some repository, soon after the first published results, to expert theorists willing to extract the physical information they contain.

[1] T. Damour, B. R. Iyer and B. S. Sathyaprakash, Phys. Rev. D **57**, 885 (1998). [arXiv:gr-qc/9708034].
[2] A. Buonanno and T. Damour, Phys. Rev. D **59**, 084006 (1999). [arXiv:gr-qc/9811091].
[3] A. Buonanno and T. Damour, Phys. Rev. D **62**, 064015 (2000). [arXiv:gr-qc/0001013].
[4] T. Damour, P. Jaranowski and G. Schäfer, Phys. Rev. D **62**, 084011 (2000). [arXiv:gr-qc/0005034].
[5] T. Damour, Phys. Rev. D **64**, 124013 (2001). [arXiv:gr-qc/0103018].
[6] F. Pretorius, Phys. Rev. Lett. **95**, 121101 (2005) [arXiv:gr-qc/0507014].
[7] F. Pretorius, Class. Quant. Grav. **23**, S529 (2006) [arXiv:gr-qc/0602115].
[8] M. Campanelli, C. O. Lousto, P. Marronetti and Y. Zlochower, Phys. Rev. Lett. **96**, 111101 (2006) [arXiv:gr-qc/0511048].
[9] M. Campanelli, C. O. Lousto and Y. Zlochower, Phys. Rev. D **73**, 061501(R) (2006) [arXiv:gr-qc/0601091].
[10] M. Campanelli, C. O. Lousto and Y. Zlochower, Phys. Rev. D **74**, 041501(R) (2006) [arXiv:gr-qc/0604012].
[11] J. G. Baker, J. Centrella, D. I. Choi, M. Koppitz and J. van Meter, Phys. Rev. D **73**, 104002 (2006) [arXiv:gr-qc/0602026].
[12] J. G. Baker, J. Centrella, D. I. Choi, M. Koppitz, J. R. van Meter and M. C. Miller, Astrophys. J. **653**, L93 (2006) [arXiv:astro-ph/0603204].
[13] J. G. Baker, M. Campanelli, F. Pretorius and Y. Zlochower, Class. Quant. Grav. **24**, S25 (2007) [arXiv:gr-qc/0701016].
[14] J. A. Gonzalez, U. Sperhake, B. Brügmann, M. Hannam and S. Husa, Phys. Rev. Lett. **98**, 091101 (2007) [arXiv:gr-qc/0610154].
[15] S. Husa, J. A. Gonzalez, M. Hannam, B. Brugmann and U. Sperhake, arXiv:0706.0740 [gr-qc].
[16] M. Koppitz, D. Pollney, C. Reisswig, L. Rezzolla, J. Thornburg, P. Diener and E. Schnetter, Phys. Rev. Lett. **99**,041102 (2007) [arXiv:gr-qc/0701163].
[17] L. Rezzolla, E. N. Dorband, C. Reisswig, P. Diener, D. Pollney, E. Schnetter and B. Szilagyi, arXiv:0708.3999 [gr-qc] (2007).
[18] L. Rezzolla, P. Diener, E. N. Dorband, D. Pollney, C. Reisswig, E. Schnetter and J. Seiler, arXiv:0710.3345 [gr-qc] (2007).

[19] M. Boyle *et al.*, arXiv:0710.0158 [gr-qc].
[20] M. Boyle, D.A. Brown, L.E. Kidder,A.H. Mroué, H.P. Pfeiffer, M.A. Scheel, G.B. Cook and S.A. Teukolsky arXiv:0710.0158 [gr-qc].
[21] F. Pretorius, arXiv:0710.1338 [gr-qc].
[22] T. Damour, E. Gourgoulhon and P. Grandclement, Phys. Rev. D **66**, 024007 (2002) [arXiv:gr-qc/0204011].
[23] E. Gourgoulhon, P. Grandclement and S. Bonazzola, Phys. Rev. D **65**, 044020 (2002) [arXiv:gr-qc/0106015].
[24] P. Grandclement, E. Gourgoulhon and S. Bonazzola, Phys. Rev. D **65**, 044021 (2002) [arXiv:gr-qc/0106016].
[25] T. Damour, B. R. Iyer, P. Jaranowski and B. S. Sathyaprakash, Phys. Rev. D **67**, 064028 (2003) [arXiv:gr-qc/0211041].
[26] A. Buonanno, G. B. Cook and F. Pretorius, Phys. Rev. D **75**, 124018 (2007) [arXiv:gr-qc/0610122].
[27] Y. Pan *et al.*, arXiv:0704.1964 [gr-qc].
[28] T. Damour and A. Nagar, Phys. Rev. D **76**, 044003 (2007).
[29] A. Buonanno, Y. Pan, J. G. Baker, J. Centrella, B. J. Kelly, S. T. McWilliams and J. R. van Meter, Phys. Rev. D **76**, 104049 (2007) [arXiv:0706.3732 [gr-qc]].
[30] T. Damour and A. Nagar, Phys. Rev. D **76**, 064028 (2007) [arXiv:0705.2519 [gr-qc]].
[31] T. Regge and J.A. Wheeler, Phys. Rev. **108**, 1063 (1957).
[32] F. J. Zerilli, Phys. Rev. Lett. **24**, 737 (1970).
[33] K. Martel and E. Poisson, Phys. Rev. D **71**, 104003 (2005) [arXiv:gr-qc/0502028].
[34] A. Nagar and L. Rezzolla, Class. Quant. Grav. **22**, R167 (2005) [Erratum-ibid. **23**, 4297 (2006)] [arXiv:gr-qc/0502064].
[35] A. Nagar, T. Damour and A. Tartaglia, Class. Quant. Grav. **24**, S109 (2007) [arXiv:gr-qc/0612096].
[36] M. Davis, R. Ruffini and J. Tiomno, Phys. Rev. D **5**, 2932 (1972).
[37] M. Sasaki and H. Tagoshi, Living Rev. Relativity **6**, (2003), 6. URL (cited on January 22, 2008) http://www.livingreviews.org/lrr-2003-6.
[38] C. Cutler, L. S. Finn, E. Poisson and G. J. Sussman Phys. Rev. D **47**, 1511 (1993).
[39] E. Poisson, Phys. Rev. D **52**, 5719 (1995) [Addendum-ibid. D **55**, 7980 (1997)] [arXiv:gr-qc/9505030].
[40] H. Tagoshi and M. Sasaki, Prog. Theor. Phys. **92**, 745

(1994) [arXiv:gr-qc/9405062].

[41] L. E. Kidder, arXiv:0710.0614 [gr-qc].

[42] E. Berti, V. Cardoso, J. A. Gonzalez, U. Sperhake, M. Hannam, S. Husa and B. Bruegmann, Phys. Rev. D **76**, 064034 (2007) [arXiv:gr-qc/0703053].

[43] T. Damour and A. Gopakumar, Phys. Rev. D **73**, 124006 (2006) [arXiv:gr-qc/0602117].

[44] L. Blanchet and T. Damour, Phil. Trans. Roy. Soc. Lond. A **320**, 379 (1986).

[45] L. Blanchet, Proc. Roy. Soc. Lond. A **409**, 383 (1987).

[46] L. Blanchet and T. Damour, Annales Institut H. Poincaré, Phys. Theor. **50**, 377 (1989).

[47] T. Damour and B. R. Iyer, Phys. Rev. D **43**, 3259 (1991).

[48] T. Damour and B. R. Iyer, Annales Institut H. Poincaré, Phys. Theor. **54**, 115 (1991).

[49] L. Blanchet and T. Damour, Phys. Rev. D **46**, 4304 (1992).

[50] L. Blanchet, Class. Quant. Grav. **15**, 113 (1998) [Erratum-ibid. **22**, 3381 (2005)]. [arXiv:gr-qc/9710038].

[51] L. Blanchet, T. Damour, B. R. Iyer, C. M. Will and A. G. Wiseman, Phys. Rev. Lett. **74**, 3515 (1995) [arXiv:gr-qc/9501027].

[52] L. Blanchet, B. R. Iyer and B. Joguet, Phys. Rev. D **65**, 064005 (2002) [Erratum-ibid. D **71**, 129903 (2005)]. [arXiv:gr-qc/0105098].

[53] L. Blanchet, T. Damour, G. Esposito-Farese and B. R. Iyer, Phys. Rev. Lett. **93**, 091101 (2004). [arXiv:gr-qc/0406012].

[54] L. Blanchet, T. Damour, G. Esposito-Farese and B. R. Iyer, Phys. Rev. D **71**, 124004 (2005) [arXiv:gr-qc/0503044].

[55] L. Blanchet, G. Faye, B. R. Iyer and B. Joguet, Phys. Rev. D **65**, 061501 (2002) [Erratum-ibid. D **71**, 129902 (2005)] [arXiv:gr-qc/0105099].

[56] T. Tanaka, H. Tagoshi and M. Sasaki, Prog. Theor. Phys. **96**, 1087 (1996) [arXiv:gr-qc/9701050].

[57] L. E. Kidder, L. Blanchet and B. R. Iyer, Class. Quant. Grav. **24**, 5307 (2007) [arXiv:0706.0726 [gr-qc]].

[58] A. Buonanno, Y. Chen and T. Damour, Phys. Rev. D **74**, 104005 (2006) [arXiv:gr-qc/0508067].

[59] M. Hannam, S. Husa, U. Sperhake, B. Brugmann and J. A. Gonzalez, arXiv:0706.1305 [gr-qc].

[60] T. Damour, B. R. Iyer and B. S. Sathyaprakash, Phys. Rev. D **63**, 044023 (2001) [Erratum-ibid. D **72**, 029902 (2005)] [arXiv:gr-qc/0010009].

[61] J. G. Baker, J. R. van Meter, S. T. McWilliams, J. Centrella and B. J. Kelly, Phys. Rev. Lett. **99**, 181101 (2007) [arXiv:gr-qc/0612024].

[62] K. G. Arun, L. Blanchet, B. R. Iyer and M. S. S. Qusailah, Class. Quant. Grav. **21**, 3771 (2004) [Erratum-ibid. **22**, 3115 (2005)] [arXiv:gr-qc/0404085].